NIH Public Access
Author Manuscript
Magn Reson Imaging Clin N Am. Author manuscript; available in PMC 2013 November 01.

Published in final edited form as:
Magn Reson Imaging Clin N Am. 2012 November ; 20(4): 699–713. doi:10.1016/j.mric.2012.07.007.

Advanced Techniques Using Contrast Media in Neuroimaging

Jean-Christophe Ferré[a,b], **Mark S. Shiroishi**[a], and **Meng Law**[a]

[a]Division of Neuroradiology, Department of Radiology, Keck Medical Center of University of Southern California, 1520 San Pablo Street, Los Angeles, CA 90033, USA

[b]CHU Rennes, Department of Radiology, University Hospital, 2 rue Henri Le Guilloux, Rennes, France

Abstract

This article presents an overview of advanced MRI techniques using contrast media in neuroimaging, focusing on T2*-weighted dynamic susceptibility contrast MR imaging (DSC-MRI) and T1-weighted dynamic contrast-enhanced MR imaging (DCE-MRI). Image acquisition and data processing methods as well as their clinical application in brain tumors, stroke, dementia and multiple sclerosis are discussed.

Keywords

Perfusion; Permeability; Contrast agent; Brain tumor; Stroke

Introduction

Contrast agent injection is essential to characterize abnormalities in neuroimaging (see theprevious articles in this issue). However, contrast-enhancement is non-specific reflection of blood brain barrier (BBB) disruption. The injection of gadolinium-based contrast agents (GBCAs) allows characterization of the brain's hemodynamic processes - brain perfusion- and the BBB leakage-permeability. It is now recognized that advance MR imaging

© 2012 Elsevier Inc. All rights reserved.

Corresponding Author: Jean-Christophe Ferré MD, PhD, Division of Neuroradiology, Department of Radiology, Keck Medical Center of University of Southern California, 1520 San Pablo Street, Los Angeles, CA 90033, USA, Phone: (323) 226-7425, Fax: (323) 226-4059, Jean-christophe.ferre@chu-rennes.fr.

Co-authors:

Mark S. Shiroishi, MD, Assistant Professor, Division of Neuroradiology, Department of Radiology, Keck Medical Center of University of Southern California, 1520 San Pablo Street, Los Angeles, CA 90033, USA, Phone: (323) 226-7425, Fax: (323) 226-4059, Mark.Shiroishi@med.usc.edu

Meng Law MD, MBBS, FRACR, Professor of Radiology and Neurological Surgery, Division of Neuroradiology, Department of Radiology, Keck Medical Center of University of Southern California, 1520 San Pablo Street, Los Angeles, CA 90033, USA, Phone: (323) 226-7425, Fax: (323) 226-4059, Meng.Law@med.usc.edu

Publisher's Disclaimer: This is a PDF file of an unedited manuscript that has been accepted for publication. As a service to our customers we are providing this early version of the manuscript. The manuscript will undergo copyediting, typesetting, and review of the resulting proof before it is published in its final citable form. Please note that during the production process errors may be discovered which could affect the content, and all legal disclaimers that apply to the journal pertain.

DISCLOSURES

Conflict of Interest:

Dr Ferré: none

Dr Shiroishi: Consultant, Bayer Healthcare

Dr Law serves on the scientific advisory boards for Bayer HealthCare, Toshiba Medical, has received speaker honoraria from Siemens Medical Solutions, iCAD Inc, Bayer HealthCare, Bracco, Prism Clinical Imaging

NIH-PA Author Manuscript
NIH-PA Author Manuscript
NIH-PA Author Manuscript

NIH-PA Author Manuscript

NIH-PA Author Manuscript

NIH-PA Author Manuscript

techniques, such as those used to study perfusion and permeability, provide physiologic rather than simply morphologic data obtained with conventional MRI (1).

Dynamic contrast imaging could be separate in two main categories according to the contrast agent properties: the dynamic susceptibility contrast imaging (DSC-MRI) using T2- or T2*- weighted imaging and the dynamic relaxivity contrast-enhanced MRI imaging (DCE-MRI) using T1-weighted relaxivity imaging. Both perfusion and permeability measurements could be extracted from these two technique categories, but DSC-MRI is commonly referred to as “perfusion” imaging and DCE-MRI is commonly referred to as “permeability” imaging. DSC-MRI is the most utilized technique in clinical imaging of brain tumor and stroke. This technique can provide hemodynamic metrics such as cerebral blood flow (CBF), cerebral blood volume (CBV), and mean transit time (MTT). Compared to DSC-MRI, DCE-MRI has experienced relatively less widespread use, likely owing to more stringent acquisition and complex requirements to explore BBB permeability.

The aim of this review is to give an overview of the basic principles and common neuroimaging applications of these two advanced techniques using contrast media.

Imaging Technique

Perfusion: DSC-MRI

Principle—DSC-MRI, also known as perfusion-weighted MR imaging (PWI), MR perfusion (MRP) or bolus-tracking MRI, is a technique to track the first-pass of an exogenous, paramagnetic, non-diffusible contrast agent, typically a GBCA through the tissue. Since it was first described by Villringer et al. in 1988 (2), DSC-MRI has emerged as a dominant method to study the brain microvascular component. To record the signal loss due to susceptibility effects during the first passage of a GBCA through the tissue of interest, T2 or T2*-weighted images should be dynamically acquired at a rate faster than the time it takes the bolus to pass through the tissue. With the application of tracer kinetic models for intravascular tracers and the use of the central volume theorem, the major perfusion parameters cerebral blood volume (CBV), cerebral blood flow (CBF) and mean transit time (MTT), can be estimated (Figure 1) (3,4).

Images acquisition—A single-shot echo planar imaging (EPI) is generally used because it provides a means for very rapid image acquisition. EPI is generally performed in conjunction with multislice gradient-echo (GRE) or spin echo (SE)-EPI techniques. GRE-EPI methods (T2*-weighted images) are able to provide better spatial coverage of the brain, are sensitive to both large and small vessels with better signal-to-noise ratio, and require half the dose of a GBCA compared with multislice SE (T2-weighted images). Compared with GRE, SE techniques appear to be more sensitive to smaller vessels (capillaries) and have less image distortion and artifacts at the brain-bone interface (5,6). Despite these advantages, studies have borne out that GRE sequences are superior in their ability to predict glioma grade than SE sequences (7,8). Even if combination of both techniques have been reported (6), the GRE-EPI method is the most widely utilized technique. Both 2D EPI and 3D sequences are used, however, 2D sequences are usually preferred compared because of their ability to achieve better spatial resolution, shorter TRs and provide a more accurate characterization of bolus passage (9). The typical acquisition time for the first pass T2* DSC MRI acquisition is on the order of 90 seconds. A temporal resolution on the order of 1-2 seconds is desired to obtain the correct shape of the concentration-time curve. The recommended matrix resolution is 128 × 128. Slice thickness could range between 2 to 5 mm depending on the need for whole brain volume coverage. A combination of a phase-array coil and parallel imaging, in particular at 3T, offers a good compromise in the quality of images (10).

NIH-PA Author Manuscript

NIH-PA Author Manuscript

NIH-PA Author Manuscript

Injection protocol—A GBCA bolus injection should commence within 20 seconds after the start of the T2* DSC sequence to establish a precontrast baseline. A power injector is used to inject at a minimum rate of 4 mL/sec, followed by a saline flush at the same rate, through an 18–22 gauge peripheral intravenous line. A 0.1 mmol/kg dose of GBCA is generally recommended. When the possibility of contrast agent extravasation exists, i.e. evaluation of brain tumors, a preload-correction approach is recommended (11). While the optimal amount of pre-load dosing of GBCA is not entirely clear, work by Hu et al. found that at 3T, pre-load dose of 0.1 mmol/kg administered 6 minutes before the DSC acquisition injection appeared to provide correction for leakage effects and to obtain the highest accuracy of CBV (12). If combined permeability and perfusion MRI is being performed, then it is recommended that the dose be split into 2 equivalent 0.05 mmol/kg doses (13).

There is no clear consensus in the choice of Gd contrast agent. High relaxivity contrast agents such as gadobenate dimeglumine allows high-quality (rCBV) maps (14). Gadobenate dimeglumine and high concentration GBCA gadobutrol give similar high-quality perfusion maps at dose of 0.1 mmol/kg at 1.5T (15). Whereas at 3T, gadobutrol seems to offer advantages over gadobenate dimeglumine (16). A recent study concluded that DSC-MRI with a blood pool agent such as ferumoxytol may provide a better monitor of tumor rCBV than DSC-MRI with gadoteridol (17).

Image processing—First, the GBCA concentration-time curve is calculated based on the susceptibility signal intensity-time curve. GBCA concentration is assumed to be proportional to the change in relaxation rate $\Delta R2^*$ (or $\Delta R2$ if SE sequence is used) which can be calculated from the signal intensity (18) via the equation (1):

$$\Delta R2^* = [-\ln(S(t)/S0]/TE \quad (1)$$

Where S(t) is the signal intensity in the voxel at time t and S0 is the baseline signal intensity before the bolus arrives.

A gamma-variate function is then generally fitted to the curve to eliminate contribution of tracer recirculation (19).

The most common processing methods used in clinical work give **qualitative** parametric maps assuming a constant arterial input function in all the pixels. rCBV (is calculated from the area under the curve, rMTT from the first moment of the measured efflux concentration-time curve (i.e. the weighted arithmetic mean of the time values represented in the concentration-time curve), and rCBF equal to rCBV/rMTT according to the central volume principle (20). These maps do not afford quantitative assessment of brain hemodynamics, but provide indicators of hemodynamic disturbances that are very useful in a clinical setting. They can be interpreted visually or semi-quantitatively by calculating the ratio or difference between the values in a ROI placed in the abnormal area and a contralateral ROI placed in the area considered as a normal reference.

To **quantitatively** determine CBF (mL/100 g/min) and MTT (sec), the arterial input function (AIF) must be known to correct for bolus delay and dispersion. Following deconvolution of the concentration-time curve with the AIF, MTT and CBF can be determined from the tissue residue function: CBF is the peak of the residue function and MTT is the weighted arithmetic mean of the time of transit values (20–22). CBV (in mL/100g) is then equal to CBF × MTT according to the central volume principle.

As opposed to the relationship between attenuation and contrast agent concentration in CT perfusion, there may not always exist a linear relationship between MR signal intensity and

NIH-PA Author Manuscript

NIH-PA Author Manuscript

NIH-PA Author Manuscript

tissue contrast agent concentration in DSC-MRI (23). In clinical context, this non-linear relationship is often ignored and this can lead to substantial errors in absolute quantification of DSC-MRI (24).

Permeability: DCE-MRI

Principle—DCE-MRI is employed to characterize the functional integrity of the BBB via estimation of microvascular permeability parameters. During T1-weighted DCE-MRI, the contrast agent accumulation results in T1-shortening and positive enhancement. Through pharmacokinetic modeling of contrast agent accumulation into the extravascular-extracellular space (EES), a number of parameters can be determined (Figure 1) (25):

- Transfer constant (K^{trans}), frequently called vascular permeability, is a combination of capillary wall permeability surface area product per unit volume volume of tissue (PS), and capillary blood flow (F)
- Volume of the EES per volume of tissue (v_e)
- Fractional blood-plasma volume (v_p)
- Rate constant between EES and blood plasma (k_{ep}, where $k_{ep} = K^{trans}/v_e$).

Image acquisition—Baseline T1 mapping is performed prior to the acquisition of the dynamic contrast-enhanced images. This is necessary to apply pharmacokinetic modeling because the relationship between the measured signal intensity and contrast agent concentration is non-linear (26). The most commonly used method is a multiple flip angle gradient echo acquisition but inversion or saturation recovery techniques could also be used (27,28).

Then rapid repeated T1-weighted images are acquired before, during and after bolus GBCA administration for several minutes. This is commonly performed using gradient echo sequence (SPGR, MPRAGE, VIBE) that provides adequate compromise between temporal resolution, volume coverage and sensitivity to T1 effects (29). Although 2D sequences could be used, 3D sequences are the preferred technique due to its better signal-to-noise-ratio and less severe distortions.

The acquisition time for the dynamic acquisition should be at least 3–5 minutes, and a temporal resolution of between 3.5 to 6 seconds would be optimal. The recommended matrix resolution is 128 × 128. Slice thickness could range between 2 to 7 mm depending on the need for volume coverage. To improve temporal and/or spatial resolution, parallel imaging methods or other undersampling methods, as highly constrained back-projection, or compressed sensing methods can be used (30,31).

Injection protocol—GBCA bolus injection should commence within 20 seconds after the start of the T1 DCE sequence to establish a pre-contrast baseline. A power injector is used to inject through an 18–22 gauge peripheral intravenous line, at a rate of 2 to 5 mL/sec, followed by a saline flush at the same rate. A 0.1 mmol/kg dose of contrast agent is generally recommended. If combined permeability and DSC-MRI is being performed, then it is recommended that the dose be split into two equivalent 0.05 mmol/kg doses followed by a 10 cc saline flush.

Image processing—Many methods have been described to analyse DCE-MRI, from simple measurement of MR signal changes to physiological methods using pharmacokinetic models.

NIH-PA Author Manuscript

NIH-PA Author Manuscript

NIH-PA Author Manuscript

Descriptive methods examine simple descriptions of the signal intensity-time curve like percentage of enhancement, curve shape, wash-in and wash-out slopes, or time to 90% enhancement (T90) (32). To improve reproducibility and repeatability, determination of the contrast-concentration curve could be derived from signal intensity-time curve. A simple descriptor as the initial area under the contrast agent concentration-time curve (IAUC) can be calculated without pharmacokinetic modeling. It is widely used in drug trials and appears to have fair reproducibility. However, what it represents physiologically is unclear as it is a combination of blood volume, flow, permeability and EES volume (25).

Permeability metrics can also be extracted from the concentration-time curve using **pharmacokinetic models** which in theory should limit individual patient variation, scanner type or imaging technique. Most of pharmacokinetic models applied to DCE-MRI are compartmental models. A simplification of the pharmacokinetic model was proposed by Patlak et al., to estimate K^{trans} with a graphical approach in case of limited permeability (33). Models proposed by Toft and Kernode and Larson et al. define K^{trans} (min^{-1}) and v_e neglecting the contribution of the intravascular compartment (34,35). However, when there is a large increase in blood volume, (i.e.in high grade tumor), ignoring the contribution of the intravascular tracer may be problematic (36). Extensions of this model which take into consideration the contribution the intravascular contrast have been developed that allow modeling of v_p in addition to K^{trans} and v_e. These models provide more accurate calculation of K^{trans} and v_e (37). Because K^{trans} is a composite parameter depending on the relationship between flow F and capillary permeability–surface area product (PS) more complex models, such as the adiabatic tissue homogeneity model, separate F and PS (38). However, these models demand a very high temporal resolution and a high quality of data.

An AIF is needed for the models described above. Ideally, the AIF should be determined in an artery local to the tissue of interest for each examination. But an accurate measurement is challenging (39). Several techniques have been proposed, but many groups use an idealized mathematical function, based on population-averaged AIF (35,40).

Limitations of DSC-MRI and DCE-MRI

Quantification of perfusion and permeability metrics is based on several approximations and assumptions. Moreover, many acquisition, processing, and interpretation methods are used for DSC-MRI and DCE-MRI, without standardization across centers. These imply difficulties to compare and to use the reported values in the literature.

Because the main DSC-MRI acquisition techniques are T2*-weighted methods, susceptibility artifacts can confound perfusion measurements, particularly in the posterior fossa, temporal and frontal lobes, hemorrhagic lesions and in the surgical setting where there can be blood products (13,41). Several solutions include decreasing slices thickness, and shortening TE with the use of parallel imaging (10).

T2*-weighted methods have also significant T1 sensitivity. When the BBB is disrupted, as is often the case with brain tumors, the leakage of GBCA results in enhanced T1 relaxation effects. These effects produce an elevation in the signal curve mask signal that can result in underestimation of rCBV (42,43). Acquisition method with low flip angle and short TE can minimize the T1-effets (42). Moreover, the leakage effect can be reduced using GBCA preloading to saturate the extravascular space, and mathematical correction (11,12). DCE-MRI metrics could be easily extracted in brain area with high leakage of Gd- in post-Gd enhanced part of the brain- with a relatively short acquisition time. Measuring permeability in non-enhanced brain is more challenging: a longer acquisition and an adaptation of quantification model are needed.

NIH-PA Author Manuscript

NIH-PA Author Manuscript

NIH-PA Author Manuscript

Imaging Findings/Pathology

This section will highlight the current and future potential clinical applications of DSC-MRI and DCE-MRI in neuroimaging. Several recent review articles have previously detailed uses of these techniques (13,44–46).

Brain tumor

The usefulness of DSC-MRI and DCE-MRI in brain tumor imaging is based on the detection of intratumoral microvascular abnormalities: The disorganized angiogenesis is associated with vascular permeability induced by the vascular endothelial growth factor (VEGF)-A in high grade tumor (47). CBV and K^{trans} are respectively correlated with these histopathological findings in high grade tumor (48,49).

The most widely used parameter is the rCBV ratio (tumoral rCBV /contralateral normal brain rCBV). Several different methods exist to determine the regions of interest (ROI) used to extract rCBV values. A more accurate measurement of tumoral rCBV is the maximal rCBV chosen among several ROI placed in several hot spots (50).

Differential diagnosis of intracranial lesions

Differentiation of brain abscess versus cystic brain tumor—Distinguishing a pyogenic brain abscess from a cystic brain tumor is sometimes difficult using conventional MRI where both can present as rim-enhancing masses. Diffusion imaging is very helpful to making a distinction where an abscess is classically associated with internal diffusion restriction. However small abscess and non-pyogenic abscesses, such as toxoplasmosis, can display increased diffusion (51). A few studies have demonstrated a significantly lower rCBV ratio (< 0.95) in the abscess wall than in tumor wall (Figure 2) (52,53). One study demonstrated that K^{trans} and v_e could also be helpful for this distinction (54).

Tumefactive demyelinating lesion (TDL) Versus Glioma—A TDL can appear similar to a brain tumor not only on conventional imaging, but also at histopathology where hypercellularity and atypical reactive astrocytes can mimic high grade glioma. Cha et al. have demonstrated that rCBV ratio was useful in differentiating TDL from intracranial neoplasms, with values of 0.88 and 6.47 respectively (Figure 3) (55). However, some contrast-enhanced lesions in multiple sclerosis can have an increased CBV (see below) (56).

Differentiation of Cerebral Lymphoma Versus Glioma—A lower rCBV ratio was found in primary lymphoma than in high grade glioma (Figure 4) because an important pathological finding is the tumor infiltration along the capillaries, and not an important tumor neoangiogenesis like in HGG.A threshold value of 1.2 for rCBV ratio gave a positive predictive value of 94% and a negative predictive value of 89% to differentiate these tumors (57). In this study, metrics extracted from DCE were not significantly different between lymphomas, high grade gliomas and metastases (57).

Using a BBB leakage correction algorithm, but not a GBCA preloading, Mangla et al. reported that percentage signal recovery (PSR) derived from DSC-MRI signal-time curve was superior to the rCBV ratio to differentiate lymphoma, to high grade glioma and metastasis. Mean PSR was high in lymphoma (113.1 ± 41.6), intermediate in GBM (78.2 ± 14.3), and low in metastases (53.5 ± 12.9) (58).

NIH-PA Author Manuscript

NIH-PA Author Manuscript

NIH-PA Author Manuscript

Glioma

Predicting glioma grade—Compared to biopsy or surgery, MRI has the advantage of being able to evaluate the entire glioma, as well as the surrounding brain parenchyma which is typically not resected nor biopsied. However, despite numerous shortcomings such as reproducibility and sampling error, the WHO classification remains the standard reference for predicting prognosis and guiding therapy in patients with brain tumors. Therapy for high grade glioma (HGG, WHO grade III and IV) typically consists of surgery and adjuvant chemoradiation, whereas management for low grade (LGG, WHO grade I and II) is less invasive.

Compared with conventional contrast-enhanced MRI, perfusion MR using rCBV ratio increases the sensitivity and predictive value in predicting glioma grade (59). However, reported threshold values vary due to absence of standardization for acquisition parameters and processing methods. Maximal rCBV values of LGG are ranged between 1.11 to 2.14, whereas maximal rCBV values of HGG are higher, between 3.54–7.32 (59–62). Law et al. demonstrated that a threshold value of 1.75 provides sensitivity of 95%, specificity of 57.5%, PPV of 87%, and NPV of 79.3% (Figure 4) (59).

K^{trans} derived from DCE-MRI have also been found to correlate with glioma grade and the histologic proliferative marker, MIB-1, (63). Using K^{trans} extracted from DSC-MRI, the correlation between K^{trans} and tumor grade was less important than the correlation between rCBV and tumor grade (64). However using DCE-MRI, K^{trans} has been found to discriminate LGG from HGG with a sensitivity and specificity >90% (65,66). Also, rCBV and K^{trans} were correlated for tumor grading, but regions of increased rCBV were different to regions of increased permeability, likely reflecting the heterogeneity of the glioma vasculature (64,67).

Predicting prognosis and therapeutic response—DSC-MRI and DCE-MRI can help in predicting prognostic of glioma. Bisdas et al. determined that an rCBVratio > 4.2 was predictive of recurrence and rCBV ≤ 3.8 was predictive of 1 year survival (68). In patients with HGG, Hirai *et al.* demonstrated that rCBV > 2.3 was an independent prognostic biomarker for predicting survival (69). They found that 2 year survival was significantly higher for patients with low (≤ 2.3) than with high (≥ 2.3) maximum rCBV. Cao et al. demonstrated that permeability assessed by DCE-MRI in HGG, although not a predictor for survival, was a predictor for time to progression (70). Using clinical outcome and not the WHO classification scheme as reference, Law et al. compared the value of rCBV in 189 patients with glioma (71). They show that glioma patients who have high baseline rCBV (>1.75) had a significantly more rapid time to progression than patients with low rCBV (<1.75), whatever the grade high or low (71). These results suggest that rCBV from DSC-MRI imaging may overcome some of the limitations of the current histologic methods to provide an additional prognostic factor for tumor biology.

Guiding biopsy and radiosurgery—Tumor biopsy and radiosurgery are usually guided with enhancement on post-contrast T1w images (72). The most malignant region of a tumor could be outside the enhancing of a glioma, DSC-MRI and DCE-MRI may be useful to guide the surgeon toward the most vascular and malignant portion of the mass (13).

Follow-up of brain tumor

Predicting malignant transformation of LGG—Patients with LGG often undergo regular follow-up MRI's to detect malignant transformation at the earliest stage possible. DSC-MRI perfusion imaging could be helpful. Indeed, studies have demonstrated that high rCBV (>1.75) in LGG is associated with poor prognosis (71). Moreover significant

NIH-PA Author Manuscript

NIH-PA Author Manuscript

NIH-PA Author Manuscript

increases in rCBV can be detected up to 12 months before contrast enhancement is noted on conventional post-contrast T1w images (73).

Therapeutic monitoring—DSC-MRI and DCE-MRI may help monitor treatment response and recurrence in the post-therapeutic brain because the appearance of contrast enhancement is nonspecific (1). DSC-MRI (74) and DCE-MRI could be helpful to differentiate residual or recurrent tumor from therapy induced changes as late necrosis induced by radiotherapy, pseudoprogression –early necrosis induced by combined chemoradiotherapy- or pseudoresponse- “masked” disease progression after antiangiogenic.

Delayed radiation necrosis and recurrent tumor: While recurrent tumor demonstrates increased vascular proliferation and angiogenesis, delayed radiation necrosis (DRN) is an occlusive vasculopathy. Both conditions can appear as regions contrast enhancement and sometimes both conditions can be present simultaneously rCBV is decreased and permeability is mildly elevated in DRN while in residual/recurrent tumor both rCBV and permeability are significantly elevated (13).

Several studies have demonstrated good results of DSC-MRI in the differentiation between DRN and tumor recurrence (41,75). While threshold rCBV values vary according the studies, the rCBV in DRN are lower than the rCBV of normal white matter, whereas in tumor recurrence rCBV are generally higher than the rCBV of normal white matter. Ktrans is reduced in DRN because the enhancement is typically slow, without a rapid vascular phase (13,76). On the other hand, Ktrans is elevated in recurrent tumor, in association with a very rapid initial increase in the vascular permeability curve, compatible with a rapid vascular phase (13,76).

Pseudoprogression: Pseudoprogression is an increase of size and enhancement in high-grade gliomas attributed to the use of combined chemoradiotherapy with temozolomide. This therapy induced necrosis appears in the first 3 to 6 months of treatment, and occurs more dramatically than that seen with radiotherapy alone (74,77).

The use of conventional contrast-enhanced MR to distinguish true early progression from pseudoprogression appears to be limited (78,79). Preliminary findings of pseudoprogression using DSC-MRI and DCE-MRI suggest a decrease in rCBV and a moderate increase in vascular permeability (Figure 5) (80,81).

Pseudoresponse: Antiangiogenic agents, such as bevacizumab or cediranib, are now administrated in patients with recurrent high-grade gliomas (82). The term “pseudoresponse” is applied to the rapid decrease in enhancement following treatment with anti-angiogenesis agents (83). The decreased enhancement may at least partially result from decreased vessels permeability and not necessarily from antitumor effects. Some patients clinically progress despite absence of enhancing tumor progression on MRI (82). In our preliminary experience, those patients with true response to bevacizumab appear to demonstrate a decrease in rCBV and permeability (13). The decrease of K^{trans} can be seen even after a single dose of cediranib and this effect is reversible when the drug is withdrawn (83).Using a “vascular normalization index”, including in Ktrans, microvessel volume, and circulating collagen IV was found to be associated with overall survival and progression free survival in patients given a single dose of cediranib (84).

NIH-PA Author Manuscript

NIH-PA Author Manuscript

NIH-PA Author Manuscript

Other pathologies

Stroke

Preliminary studies using DSC-MRI in acute ischemic stroke have demonstrated its usefulness in establishing diagnosis and predicting prognosis. The perfusion/diffusion mismatch -hypoperfusion volume greater than diffusion weighted imaging (DWI) ischemic lesion volume- is considered to represent the tissue at risk for infarction without arterial recanalization (85–87). Baseline volume DSC-MRI hypoperfusion demonstrates a better correlation with NIH Stroke Scale (NIHSS) at baseline or clinical outcome than the volume of DWI lesions (88,89), regardless of the perfusion parameter used, TTP (88), CBF or MTT (Figure 6) (85,86).

The most widely used therapy for acute stroke reperfusion is recombinant tissue plasminogen activator (tPA). Initially it has been proven to improve patients' outcome if it used within 3 hours or symptom onset (NINDS study) (90). More recently, the time window was extended to 4.5 hours in a select stroke population (ECASS-III study) (91). However this time window ignores the variation between individual stroke patients. Several studies demonstrated a benefit of thrombolysis outside of the usual time window up to 6 or 9 hours after clinical onset using different definition of DWI/DSC-MRI mismatch (92–95). Several perfusion thresholds were used to differentiate "at risk" versus "not at risk tissue" (96). For a wider clinical use of perfusion imaging in this context, a greater consistency of thresholds definition is needed. Using automatic software is suggested as a way to improve the determination of patient who could benefit to recanalization (45).

An early reperfusion response based on MTT has been found to be predictive of clinical recovery with standard intravenous rtPA therapy. A decrease of ≥30% in the volume of hypoperfusion on MTT maps 2 hours after treatment was a strong predictor of clinical outcome (97).

Permeability

Some studies suggested that permeability imaging may be helpful to predict hemorrhagic transformation (HT) in patients with acute ischemic stroke. In a study of10 patients with acute ischemic stroke, Kassner et al. found significantly increased permeability in 3 patients who went on to HT within 48 hours after clinical onset using DCE-MRI with the Patlak model (98). With this technique, a minimal DCE acquisition duration of 3 min 30 s seemed to be necessary to discriminate between HT and non-HT patients (99). Permeability maps extracted from DSC-MRI may also identify patients at risk for HT (100).

Dementia

DSC-MRI has been rarely used to study patient with dementia. Nuclear medicine techniques or arterial spin labeling (ASL) techniques are preferred because injection of GBCA is not recommended to evaluate dementia patients with MRI.

However, recent papers showed that reduction of flow, hypoxia, and BBB dysfunction might initiate or contribute to neuronal degeneration, notably in Alzheimer's disease (101). Some studies using MRI have shown increased BBB permeability with normal aging, and also an increased permeability in patients with vascular dementia compared with age-matched control (102). Starr et al. demonstrated no significant permeability difference for AD subjects versus control or for MCI patient versus control (103,104). However these studies used only descriptive methods to estimate permeability without calculating Ktrans or PS. Improvement of DCE MRI techniques may permit accurate estimation of permeability in the hippocampus in a near future (105).

NIH-PA Author Manuscript

NIH-PA Author Manuscript

NIH-PA Author Manuscript

Multiple Sclerosis

DSC-MRI has demonstrated an increased perfusion in acute multiple sclerosis (MS) lesions, and decreased CBF and CBV in most nonenhancing MS lesions (56). A decreased CBF was also found in normal-appearing (NA) white matter (WM) and in gray matter (GM) (106–108). Cortical hypoperfusion seems to appear early in disease progression. Deep GM hypoperfusion is found in patients with relapsing remitting and primary progressive MS and is correlated with fatigue score and neuropsychological dysfunction (107). Decreased perfusion in MS patient could be explained by the presence of lesions in GM, degeneration of axons, and neuronal loss secondary to demyelination, hypoperfusion or Wallerian degeneration. A recent study using DCE-MRI demonstrated the feasibility of DCE-MRI for the quantitative assessment of PS in normal-appearing white matter as well as in focal lesions (109).

Summary

DSC-MRI and DCE-MRI can provide imaging biomarkers that reflect brain hemodynamic processes and permeability. These techniques provide physiologic information to complement conventional contrast-enhanced MRI, and their added value is now recognized, especially in of the evaluation of brain tumors and stroke. However, standardization of acquisition and processing is needed to increase their clinical benefit and allow widespread use.

Acknowledgments

Funding sources:

Dr Ferré: French Society of Radiology (SFR) research grant, French Society of Neuroradiology (SFNR) research grant

Dr Shiroishi: GE Healthcare/RSNA Research Scholar Grant

Dr Law: NIH CTSA Grant 1UL1RR031986-01, NIH 1R21EB013456 and Bayer Healthcare

References

1. Essig M, Anzalone N, Combs SE, Dörfler À, Lee SK, Picozzi P, Rovira A, Weller M, Law M. MR imaging of neoplastic central nervous system lesions: review and recommendations for current practice. AJNR Am J Neuroradiol. 2012 May; 33(5):803–817. Epub 2011 Oct 20. Review. PubMed PMID: 22016411. [PubMed: 22016411]
2. Villringer A, Rosen BR, Belliveau JW, et al. Dynamic imaging with lanthanide chelates in normal brain: contrast due to magnetic susceptibility effects. Magn Reson Med. 1988; 6:164–174. [PubMed: 3367774]
3. Calamante F, Thomas DL, Pell GS, et al. Measuring cerebral blood flow using magnetic resonance imaging techniques. J Cereb Blood Flow Metab. 1999; 19:701–735. [PubMed: 10413026]
4. Zaharchuk G. Theoretical basis of hemodynamic MR imaging techniques to measure cerebral blood volume, cerebral blood flow, and permeability. AJNR Am J Neuroradiol. 2007; 28:1850–1858. [PubMed: 17998415]
5. Simonsen CZ, Ostergaard L, Smith DF, et al. Comparison of gradient- and spin-echo imaging: CBF, CBV, and MTT measurements by bolus tracking. J Magn Reson Imaging. 2000; 12:411–416. [PubMed: 10992308]
6. Fisel CR, Ackerman JL, Buxton RB, et al. MR contrast due to microscopically heterogeneous magnetic susceptibility: numerical simulations and applications to cerebral physiology. Magn Reson Med. 1991; 17:336–347. [PubMed: 2062208]

NIH-PA Author Manuscript

NIH-PA Author Manuscript

NIH-PA Author Manuscript

7. Donahue KM, Krouwer HG, Rand SD, et al. Utility of simultaneously acquired gradient-echo and spin-echo cerebral blood volume and morphology maps in brain tumor patients. Magn Reson Med. 2000; 43:845–853. [PubMed: 10861879]
8. Sugahara T, Korogi Y, Kochi M, et al. Perfusion-sensitive MR imaging of gliomas: comparison between gradient-echo and spin-echo echo-planar imaging techniques. AJNR Am J Neuroradiol. 2001; 22:1306–1315. [PubMed: 11498419]
9. van Gelderen P, Grandin C, Petrella JR, et al. Rapid three-dimensional MR imaging method for tracking a bolus of contrast agent through the brain. Radiology. 2000; 216:603–608. [PubMed: 10924593]
10. Lupo JM, Lee MC, Han ET, et al. Feasibility of dynamic susceptibility contrast perfusion MR imaging at 3T using a standard quadrature head coil and eight-channel phased-array coil with and without SENSE reconstruction. J Magn Reson Imaging. 2006; 24:520–529. [PubMed: 16888776]
11. Paulson ES, Schmainda KM. Comparison of dynamic susceptibility-weighted contrast-enhanced MR methods: recommendations for measuring relative cerebral blood volume in brain tumors. Radiology. 2008; 249:601–613. [PubMed: 18780827]
12. Hu LS, Baxter LC, Pinnaduwage DS, et al. Optimized preload leakage-correction methods to improve the diagnostic accuracy of dynamic susceptibility-weighted contrast-enhanced perfusion MR imaging in posttreatment gliomas. AJNR Am J Neuroradiol. 2010; 31:40–48. [PubMed: 19749223]
13. Lacerda S, Law M. Magnetic resonance perfusion and permeability imaging in brain tumors. Neuroimaging Clin N Am. 2009; 19:527–557. [PubMed: 19959004]
14. Cotton F, Hermier M. The advantage of high relaxivity contrast agents in brain perfusion. Eur Radiol. 2006; 16(Suppl 7):M16–M26. [PubMed: 18655263]
15. Essig M, Lodemann KP, Le-Huu M, et al. Intraindividual comparison of gadobenate dimeglumine and gadobutrol for cerebral magnetic resonance perfusion imaging at 1.5 T. Invest Radiol. 2006; 41:256–263. [PubMed: 16481908]
16. Giesel FL, Mehndiratta A, Risse F, et al. Intraindividual comparison between gadopentetate dimeglumine and gadobutrol for magnetic resonance perfusion in normal brain and intracranial tumors at 3 Tesla. Acta Radiol. 2009; 50:521–530. [PubMed: 19337867]
17. Gahramanov S, Raslan AM, Muldoon LL, et al. Potential for differentiation of pseudoprogression from true tumor progression with dynamic susceptibility-weighted contrast-enhanced magnetic resonance imaging using ferumoxytol vs. gadoteridol: a pilot study. Int J Radiat Oncol Biol Phys. 2011; 79:514–523. [PubMed: 20395065]
18. Rosen BR, Belliveau JW, Vevea JM, et al. Perfusion imaging with NMR contrast agents. Magn Reson Med. 1990; 14:249–265. [PubMed: 2345506]
19. Thompson HK Jr, Starmer CF, Whalen RE, et al. Indicator Transit Time Considered as a Gamma Variate. Circ Res. 1964; 14:502–515. [PubMed: 14169969]
20. Leiva-Salinas C, Provenzale JM, Kudo K, et al. The alphabet soup of perfusion CT and MR imaging: terminology revisited and clarified in five questions. Neuroradiology. 2012; 54:907–918. [PubMed: 22488209]
21. Boxerman JL, Schmainda KM, Weisskoff RM. Relative Cerebral Blood Volume Maps Corrected for Contrast Agent Extravasation Significantly Correlate with Glioma Tumor Grade, Whereas Uncorrected Maps Do Not. AJNR Am J Neuroradiol. 2006; 27:859–867. [PubMed: 16611779]
22. Smith AM, Grandin CB, Duprez T, et al. Whole brain quantitative CBF, CBV, and MTT measurements using MRI bolus tracking: implementation and application to data acquired from hyperacute stroke patients. J Magn Reson Imaging. 2000; 12:400–410. [PubMed: 10992307]
23. Wintermark M, Sesay M, Barbier E, et al. Comparative overview of brain perfusion imaging techniques. Stroke. 2005; 36:e83–e99. [PubMed: 16100027]
24. Knutsson L, Stahlberg F, Wirestam R. Absolute quantification of perfusion using dynamic susceptibility contrast MRI: pitfalls and possibilities. MAGMA. 2010; 23:1–21. [PubMed: 19960361]
25. Tofts PS, Brix G, Buckley DL, et al. Estimating kinetic parameters from dynamic contrast-enhanced T(1)-weighted MRI of a diffusable tracer: standardized quantities and symbols. J Magn Reson Imaging. 1999; 10:223–232. [PubMed: 10508281]

NIH-PA Author Manuscript

NIH-PA Author Manuscript

NIH-PA Author Manuscript

26. Evelhoch JL. Key factors in the acquisition of contrast kinetic data for oncology. J Magn Reson Imaging. 1999; 10:254–259. [PubMed: 10508284]
27. Gowland P, Mansfield P, Bullock P, et al. Dynamic studies of gadolinium uptake in brain tumors using inversion-recovery echo-planar imaging. Magn Reson Med. 1992; 26:241–258. [PubMed: 1513249]
28. Parker GJ, Suckling J, Tanner SF, et al. Probing tumor microvascularity by measurement, analysis and display of contrast agent uptake kinetics. J Magn Reson Imaging. 1997; 7:564–574. [PubMed: 9170043]
29. Brookes JA, Redpath TW, Gilbert FJ, et al. Accuracy of T1 measurement in dynamic contrast-enhanced breast MRI using two- and three-dimensional variable flip angle fast low-angle shot. J Magn Reson Imaging. 1999; 9:163–171. [PubMed: 10077009]
30. Lebel, R.; Jones, J.; Ferré, JC., et al. Highly accelerated dynamic contrast enhanced imaging with prospective undersampling; 2012 May 5th–11th; Melbourne.
31. Smith DS, Welch EB, Li X, et al. Quantitative effects of using compressed sensing in dynamic contrast enhanced MRI. Phys Med Biol. 2011; 56:4933–4946. [PubMed: 21772079]
32. Daniel BL, Yen YF, Glover GH, et al. Breast disease: dynamic spiral MR imaging. Radiology. 1998; 209:499–509. [PubMed: 9807580]
33. Patlak CS, Blasberg RG, Fenstermacher JD. Graphical evaluation of blood-to-brain transfer constants from multiple-time uptake data. J Cereb Blood Flow Metab. 1983; 3:1–7. [PubMed: 6822610]
34. Larsson HB, Stubgaard M, Frederiksen JL, et al. Quantitation of blood-brain barrier defect by magnetic resonance imaging and gadolinium-DTPA in patients with multiple sclerosis and brain tumors. Magn Reson Med. 1990; 16:117–131. [PubMed: 2255233]
35. Tofts PS, Kermode AG. Measurement of the blood-brain barrier permeability and leakage space using dynamic MR imaging. 1. Fundamental concepts. Magn Reson Med. 1991; 17:357–367. [PubMed: 2062210]
36. Gaustad JV, Brurberg KG, Simonsen TG, et al. Tumor vascularity assessed by magnetic resonance imaging and intravital microscopy imaging. Neoplasia. 2008; 10:354–362. [PubMed: 18392132]
37. Tofts PS. Modeling tracer kinetics in dynamic Gd-DTPA MR imaging. J Magn Reson Imaging. 1997; 7:91–101. [PubMed: 9039598]
38. St Lawrence KS, Lee TY. An adiabatic approximation to the tissue homogeneity model for water exchange in the brain: I. Theoretical derivation. J Cereb Blood Flow Metab. 1998; 18:1365–1377. [PubMed: 9850149]
39. Paldino MJ, Barboriak DP. Fundamentals of quantitative dynamic contrast-enhanced MR imaging. Magn Reson Imaging Clin N Am. 2009; 17:277–289. [PubMed: 19406359]
40. Schabel MC, Fluckiger JU, DiBella EV. A model-constrained Monte Carlo method for blind arterial input function estimation in dynamic contrast-enhanced MRI: I. Simulations. Phys Med Biol. 2010; 55:4783–4806. [PubMed: 20679691]
41. Cha S, Knopp EA, Johnson G, et al. Intracranial mass lesions: dynamic contrastenhanced susceptibility-weighted echo-planar perfusion MR imaging. Radiology. 2002; 223:11–29. [PubMed: 11930044]
42. Kassner A, Annesley DJ, Zhu XP, et al. Abnormalities of the contrast re-circulation phase in cerebral tumors demonstrated using dynamic susceptibility contrast-enhanced imaging: a possible marker of vascular tortuosity. J Magn Reson Imaging. 2000; 11:103–113. [PubMed: 10713941]
43. Quarles CC, Schmainda KM. Assessment of the morphological and functional effects of the anti-angiogenic agent SU11657 on 9L gliosarcoma vasculature using dynamic susceptibility contrast MRI. Magn Reson Med. 2007; 57:680–687. [PubMed: 17390352]
44. Copen WA, Schaefer PW, Wu O. MR perfusion imaging in acute ischemic stroke. Neuroimaging Clin N Am. 2011; 21:259–283. x. [PubMed: 21640299]
45. Grigoryan M, Tung CE, Albers GW. Role of diffusion and perfusion MRI in selecting patients for reperfusion therapies. Neuroimaging Clin N Am. 2011; 21:247–257. ix-x. [PubMed: 21640298]
46. Shiroishi MS, Habibi M, Rajderkar D, et al. Perfusion and permeability MR imaging of gliomas. Technol Cancer Res Treat. 2011; 10:59–71. [PubMed: 21214289]

NIH-PA Author Manuscript

NIH-PA Author Manuscript

NIH-PA Author Manuscript

47. Vajkoczy P, Menger MD. Vascular microenvironment in gliomas. J Neurooncol. 2000; 50:99–108. [PubMed: 11245285]
48. Provenzale JM, Wang GR, Brenner T, et al. Comparison of permeability in high-grade and low-grade brain tumors using dynamic susceptibility contrast MR imaging. AJR Am J Roentgenol. 2002; 178:711–716. [PubMed: 11856703]
49. Roberts HC, Roberts TP, Brasch RC, et al. Quantitative measurement of microvascular permeability in human brain tumors achieved using dynamic contrast-enhanced MR imaging: correlation with histologic grade. AJNR Am J Neuroradiol. 2000; 21:891–899. [PubMed: 10815665]
50. Wetzel SG, Cha S, Johnson G, et al. Relative cerebral blood volume measurements in intracranial mass lesions: interobserver and intraobserver reproducibility study. Radiology. 2002; 224:797–803. [PubMed: 12202717]
51. Camacho DL, Smith JK, Castillo M. Differentiation of toxoplasmosis and lymphoma in AIDS patients by using apparent diffusion coefficients. AJNR Am J Neuroradiol. 2003; 24:633–637. [PubMed: 12695194]
52. Chiang IC, Hsieh TJ, Chiu ML, et al. Distinction between pyogenic brain abscess and necrotic brain tumour using 3-tesla MR spectroscopy, diffusion and perfusion imaging. Br J Radiol. 2009; 82:813–820. [PubMed: 19470568]
53. Holmes TM, Petrella JR, Provenzale JM. Distinction between cerebral abscesses and high-grade neoplasms by dynamic susceptibility contrast perfusion MRI. AJR Am J Roentgenol. 2004; 183:1247–1252. [PubMed: 15505287]
54. Haris M, Gupta RK, Singh A, et al. Differentiation of infective from neoplastic brain lesions by dynamic contrast-enhanced MRI. Neuroradiology. 2008; 50:531–540. [PubMed: 18379766]
55. Cha S, Pierce S, Knopp EA, et al. Dynamic contrast-enhanced T2*-weighted MR imaging of tumefactive demyelinating lesions. AJNR Am J Neuroradiol. 2001; 22:1109–1116. [PubMed: 11415906]
56. Ge Y, Law M, Johnson G, et al. Dynamic susceptibility contrast perfusion MR imaging of multiple sclerosis lesions: characterizing hemodynamic impairment and inflammatory activity. AJNR Am J Neuroradiol. 2005; 26:1539–1547. [PubMed: 15956527]
57. Weber MA, Zoubaa S, Schlieter M, et al. Diagnostic performance of spectroscopic and perfusion MRI for distinction of brain tumors. Neurology. 2006; 66:1899–1906. [PubMed: 16801657]
58. Mangla R, Kolar B, Zhu T, et al. Percentage signal recovery derived from MR dynamic susceptibility contrast imaging is useful to differentiate common enhancing malignant lesions of the brain. AJNR Am J Neuroradiol. 2011; 32:1004–1010. [PubMed: 21511863]
59. Law M, Yang S, Wang H, et al. Glioma grading: sensitivity, specificity, and predictive values of perfusion MR imaging and proton MR spectroscopic imaging compared with conventional MR imaging. AJNR Am J Neuroradiol. 2003; 24:1989–1998. [PubMed: 14625221]
60. Aronen HJ, Perkio J. Dynamic Susceptibility Contrast MRI of Gliomas. Neuroimaging Clin N Am. 2002; 12:501–523. [PubMed: 12687908]
61. Law M, Teicher N, Zagzag D, et al. Dynamic Contrast Enhanced Perfusion MRI in Mycosis Fungoides. J Magn Reson Imaging. 2003; 18:364–367. [PubMed: 12938134]
62. Shin JH, Lee HK, Kwun BD, et al. Using Relative Cerebral Blood Flow and Volume to Evaluate the Histopathologic Grade of Cerebral Gliomas: Preliminary Results. AJR Am J Roentgenol. 2002; 179:783–789. [PubMed: 12185064]
63. Roberts HC, Roberts TP, Bollen AW, et al. Correlation of microvascular permeability derived from dynamic contrast-enhanced MR imaging with histologic grade and tumor labeling index: a study in human brain tumors. Acad Radiol. 2001; 8:384–391. [PubMed: 11345268]
64. Law M, Yang S, Babb JS, et al. Comparison of cerebral blood volume and vascular permeability from dynamic susceptibility contrast-enhanced perfusion MR imaging with glioma grade. AJNR Am J Neuroradiol. 2004; 25:746–755. [PubMed: 15140713]
65. Nguyen TB, Cron GO, Mercier JF, et al. Diagnostic Accuracy of Dynamic Contrast- Enhanced MR Imaging Using a Phase-Derived Vascular Input Function in the Preoperative Grading of Gliomas. AJNR Am J Neuroradiol. 2012

NIH-PA Author Manuscript

NIH-PA Author Manuscript

NIH-PA Author Manuscript

66. Patankar TF, Haroon HA, Mills SJ, et al. Is volume transfer coefficient (K(trans)) related to histologic grade in human gliomas? AJNR Am J Neuroradiol. 2005; 26:2455–2465. [PubMed: 16286385]

67. Lupo JM, Cha S, Chang SM, et al. Dynamic susceptibility-weighted perfusion imaging of high-grade gliomas: characterization of spatial heterogeneity. AJNR Am J Neuroradiol. 2005; 26:1446–1454. [PubMed: 15956514]

68. Bisdas S, Kirkpatrick M, Giglio P, et al. Cerebral blood volume measurements by perfusion-weighted MR imaging in gliomas: ready for prime time in predicting shortterm outcome and recurrent disease? AJNR Am J Neuroradiol. 2009; 30:681–688. [PubMed: 19179427]

69. Hirai T, Murakami R, Nakamura H, et al. Prognostic value of perfusion MR imaging of high-grade astrocytomas: long-term follow-up study. AJNR Am J Neuroradiol. 2008; 29:1505–1510. [PubMed: 18556364]

70. Cao Y, Nagesh V, Hamstra D, et al. The extent and severity of vascular leakage as evidence of tumor aggressiveness in high-grade gliomas. Cancer Res. 2006; 66:8912–8917. [PubMed: 16951209]

71. Law M, Young RJ, Babb JS, et al. Gliomas: predicting time to progression or survival with cerebral blood volume measurements at dynamic susceptibility-weighted contrast-enhanced perfusion MR imaging. Radiology. 2008; 247:490–498. [PubMed: 18349315]

72. Kelly PJ, Daumas-Duport C, Kispert DB, et al. Imaging-based stereotaxic serial biopsies in untreated intracranial glial neoplasms. J Neurosurg. 1987; 66:865–874. [PubMed: 3033172]

73. Danchaivijitr N, Waldman AD, Tozer DJ, et al. Low-grade gliomas: do changes in rCBV measurements at longitudinal perfusion-weighted MR imaging predict malignant transformation? Radiology. 2008; 247:170–178. [PubMed: 18372467]

74. Clarke JL, Chang S. Pseudoprogression and pseudoresponse: challenges in brain tumor imaging. Curr Neurol Neurosci Rep. 2009; 9:241–246. [PubMed: 19348713]

75. Hu LS, Baxter LC, Smith KA, et al. Relative cerebral blood volume values to differentiate high-grade glioma recurrence from posttreatment radiation effect: direct correlation between image-guided tissue histopathology and localized dynamic susceptibility-weighted contrast-enhanced perfusion MR imaging measurements. AJNR Am J Neuroradiol. 2009; 30:552–558. [PubMed: 19056837]

76. Hazle JD, Jackson EF, Schomer DF, et al. Dynamic imaging of intracranial lesions using fast spin-echo imaging: differentiation of brain tumors and treatment effects. J Magn Reson Imaging. 1997; 7:1084–1093. [PubMed: 9400853]

77. Hygino da Cruz LC Jr, Rodriguez I, Domingues RC, et al. Pseudoprogression and pseudoresponse: imaging challenges in the assessment of posttreatment glioma. AJNR Am J Neuroradiol. 2011; 32:1978–1985. [PubMed: 21393407]

78. Gupta A, Shah A, Young R, et al. Pseudoprogression and the Macdonald response criteria in patients with glioblastoma. Proceedings of the Radiological Society of North America. 2009

79. Young RJ, Gupta A, Shah AD, et al. Potential utility of conventional MRI signs in diagnosing pseudoprogression in glioblastoma. Neurology. 2011; 76:1918–1924. [PubMed: 21624991]

80. Law M, Lacerda S, Shiroishi MS, et al. Characterization of disease progression versus pseudoprogression after concomitant radiochemotherapy treatment using perfusion, permeability, and MR spectroscopy in high grade gliomas. Proceedings of the Radiological Society of North America. 2009

81. Meyzer C, Dhermain F, Ducreux D, et al. A case report of pseudoprogression followed by complete remission after proton-beam irradiation for a low-grade glioma in a teenager: the value of dynamic contrast-enhanced MRI. Radiat Oncol. 2010; 5:9. [PubMed: 20132555]

82. Norden AD, Drappatz J, Muzikansky A, et al. An exploratory survival analysis of anti-angiogenic therapy for recurrent malignant glioma. J Neurooncol. 2009; 92:149–155. [PubMed: 19043778]

83. Batchelor TT, Sorensen AG, di Tomaso E, et al. AZD2171, a pan-VEGF receptor tyrosine kinase inhibitor, normalizes tumor vasculature and alleviates edema in glioblastoma patients. Cancer Cell. 2007; 11:83–95. [PubMed: 17222792]

NIH-PA Author Manuscript

NIH-PA Author Manuscript

NIH-PA Author Manuscript

84. Sorensen AG, Batchelor TT, Zhang WT, et al. A "vascular normalization index" as potential mechanistic biomarker to predict survival after a single dose of cediranib in recurrent glioblastoma patients. Cancer Res. 2009; 69:5296–5300. [PubMed: 19549889]
85. Baird AE, Benfield A, Schlaug G, et al. Enlargement of human cerebral ischemic lesion volumes measured by diffusion-weighted magnetic resonance imaging. Ann Neurol. 1997; 41:581–589. [PubMed: 9153519]
86. Barber PA, Darby DG, Desmond PM, et al. Prediction of stroke outcome with echoplanar perfusion- and diffusion-weighted MRI. Neurology. 1998; 51:418–426. [PubMed: 9710013]
87. Tong DC, Yenari MA, Albers GW, et al. Correlation of perfusion- and diffusionweighted MRI with NIHSS score in acute (<6.5 hour) ischemic stroke. Neurology. 1998; 50:864–870. [PubMed: 9566364]
88. Beaulieu C, de Crespigny A, Tong DC, et al. Longitudinal magnetic resonance imaging study of perfusion and diffusion in stroke: evolution of lesion volume and correlation with clinical outcome. Ann Neurol. 1999; 46:568–578. [PubMed: 10514093]
89. Fink JN, Selim MH, Kumar S, et al. Is the association of National Institutes of Health Stroke Scale scores and acute magnetic resonance imaging stroke volume equal for patients with right- and left-hemisphere ischemic stroke? Stroke. 2002; 33:954–958. [PubMed: 11935043]
90. Tissue plasminogen activator for acute ischemic stroke. The National Institute of Neurological Disorders and Stroke rt-PA Stroke Study Group. N Engl J Med. 1995; 333:1581–1587. [PubMed: 7477192]
91. Bluhmki E, Chamorro A, Davalos A, et al. Stroke treatment with alteplase given 3.0- 4.5 h after onset of acute ischaemic stroke (ECASS III): additional outcomes and subgroup analysis of a randomised controlled trial. Lancet Neurol. 2009; 8:1095–1102. [PubMed: 19850525]
92. Albers GW, Thijs VN, Wechsler L, et al. Magnetic resonance imaging profiles predict clinical response to early reperfusion: the diffusion and perfusion imaging evaluation for understanding stroke evolution (DEFUSE) study. Ann Neurol. 2006; 60:508–517. [PubMed: 17066483]
93. Davis SM, Donnan GA, Parsons MW, et al. Effects of alteplase beyond 3 h after stroke in the Echoplanar Imaging Thrombolytic Evaluation Trial (EPITHET): a placebo-controlled randomised trial. Lancet Neurol. 2008; 7:299–309. [PubMed: 18296121]
94. Furlan AJ, Eyding D, Albers GW, et al. Dose Escalation of Desmoteplase for Acute Ischemic Stroke (DEDAS): evidence of safety and efficacy 3 to 9 hours after stroke onset. Stroke. 2006; 37:1227–1231. [PubMed: 16574922]
95. Hacke W, Albers G, Al-Rawi Y, et al. The Desmoteplase in Acute Ischemic Stroke Trial (DIAS): a phase II MRI-based 9-hour window acute stroke thrombolysis trial with intravenous desmoteplase. Stroke. 2005; 36:66–73. [PubMed: 15569863]
96. Dani KA, Thomas RG, Chappell FM, et al. Systematic review of perfusion imaging with computed tomography and magnetic resonance in acute ischemic stroke: heterogeneity of acquisition and postprocessing parameters: a translational medicine research collaboration multicentre acute stroke imaging study. Stroke. 2011; 43:563–566. [PubMed: 21998057]
97. Chalela JA, Kang DW, Luby M, et al. Early magnetic resonance imaging findings in patients receiving tissue plasminogen activator predict outcome: Insights into the pathophysiology of acute stroke in the thrombolysis era. Ann Neurol. 2004; 55:105–112. [PubMed: 14705118]
98. Kassner A, Roberts T, Taylor K, et al. Prediction of hemorrhage in acute ischemic stroke using permeability MR imaging. AJNR Am J Neuroradiol. 2005; 26:2213–2217. [PubMed: 16219824]
99. Vidarsson L, Thornhill RE, Liu F, et al. Quantitative permeability magnetic resonance imaging in acute ischemic stroke: how long do we need to scan? Magn Reson Imaging. 2009; 27:1216–1222. [PubMed: 19695816]
100. Bang OY, Buck BH, Saver JL, et al. Prediction of hemorrhagic transformation after recanalization therapy using T2*-permeability magnetic resonance imaging. Ann Neurol. 2007; 62:170–176. [PubMed: 17683090]
101. Zlokovic BV. Neurovascular pathways to neurodegeneration in Alzheimer's disease and other disorders. Nat Rev Neurosci. 2011; 12:723–738. [PubMed: 22048062]
102. Farrall AJ, Wardlaw JM. Blood-brain barrier: ageing and microvascular disease-- systematic review and meta-analysis. Neurobiol Aging. 2009; 30:337–352. [PubMed: 17869382]

NIH-PA Author Manuscript

NIH-PA Author Manuscript

NIH-PA Author Manuscript

103. Starr JM, Farrall AJ, Armitage P, et al. Blood-brain barrier permeability in Alzheimer's disease: a case-control MRI study. Psychiatry Res. 2009; 171:232–241. [PubMed: 19211227]

104. Wang H, Golob EJ, Su MY. Vascular volume and blood-brain barrier permeability measured by dynamic contrast enhanced MRI in hippocampus and cerebellum of patients with MCI and normal controls. J Magn Reson Imaging. 2006; 24:695–700. [PubMed: 16878309]

105. Anderson VC, Lenar DP, Quinn JF, et al. The blood-brain barrier and microvascular water exchange in Alzheimer's disease. Cardiovasc Psychiatry Neurol. 2011; 2011:615829. [PubMed: 21687589]

106. Adhya S, Johnson G, Herbert J, et al. Pattern of hemodynamic impairment in multiple sclerosis: dynamic susceptibility contrast perfusion MR imaging at 3.0 T. Neuroimage. 2006; 33:1029–1035. [PubMed: 16996280]

107. Inglese M, Adhya S, Johnson G, et al. Perfusion magnetic resonance imaging correlates of neuropsychological impairment in multiple sclerosis. J Cereb Blood Flow Metab. 2008; 28:164–171. [PubMed: 17473851]

108. Law M, Saindane AM, Ge Y, et al. Microvascular abnormality in relapsing-remitting multiple sclerosis: perfusion MR imaging findings in normal-appearing white matter. Radiology. 2004; 231:645–652. [PubMed: 15163806]

109. Ingrisch M, Sourbron S, Morhard D, et al. Quantification of perfusion and permeability in multiple sclerosis: dynamic contrast-enhanced MRI in 3D at 3T. Invest Radiol. 2012; 47:252–258. [PubMed: 22373532]

NIH-PA Author Manuscript

NIH-PA Author Manuscript

NIH-PA Author Manuscript

KEY POINTS

- Studying brain perfusion and -permeability is possible without an additional dose of gadolinium-based contrast agent.
- Dynamic susceptibility contrast imaging (DSC-MRI) using T2- or T2*-weighted imaging is the most commonly used MR perfusion technique of the brain.
- Dynamic relaxivity contrast-enhanced MRI imaging (DCE-MRI) using T1-weighted relaxivity imaging is the most commonly used MR permeability technique.
- DSC-MRI and DCE-MRI can provide clinically useful physiological information to complement conventional contrast-enhanced MRI, particularly of brain tumors and stroke.

NIH-PA Author Manuscript
NIH-PA Author Manuscript
NIH-PA Author Manuscript

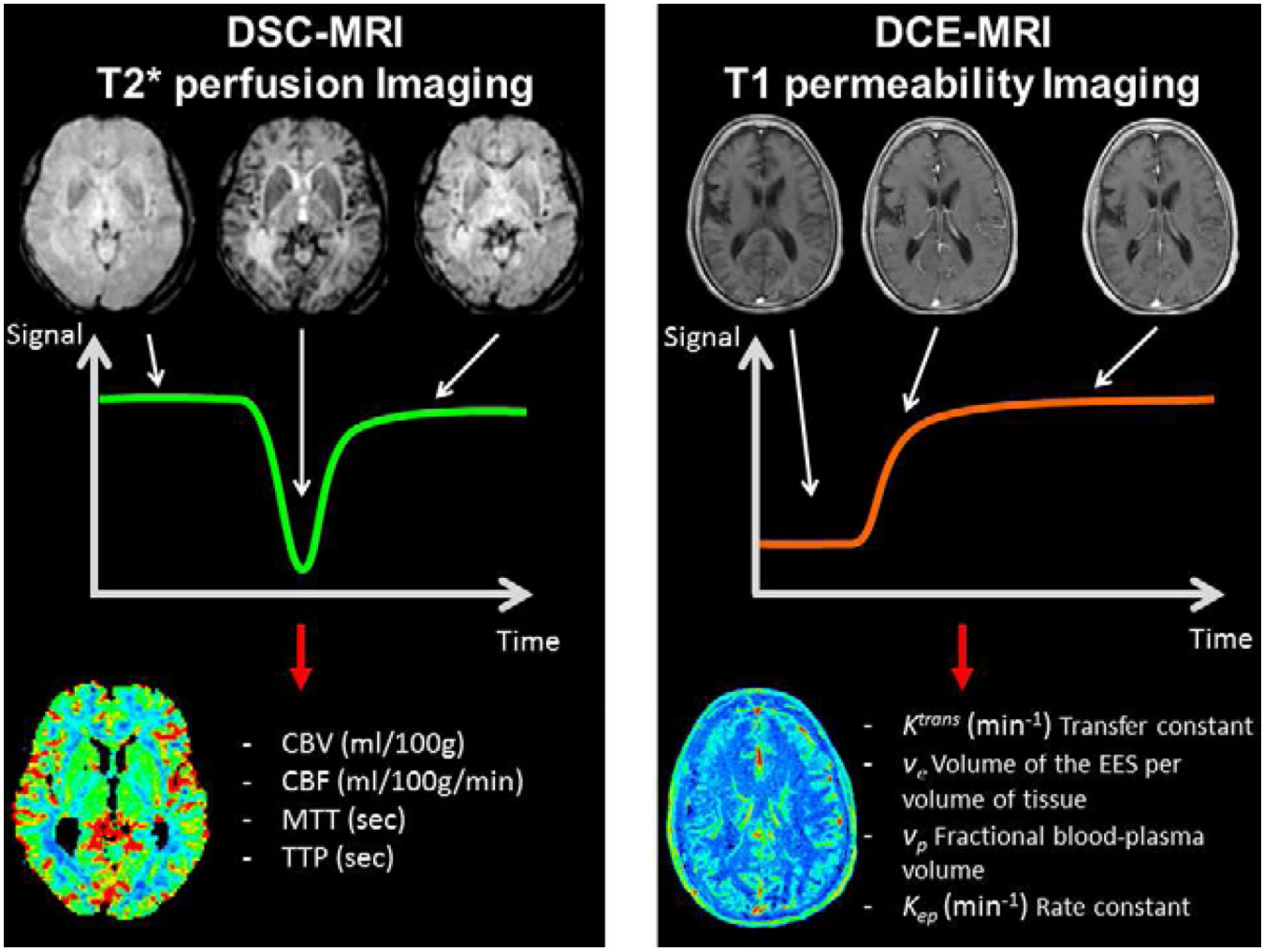

Fig. 1.

Dynamic susceptibility contrast imaging (DSC-MRI)- left column- and dynamic contrast-enhanced MRI imaging (DCE-MRI) - right column- principles overview. Sample time series images during the passage of the contrast agent - first row- and the resulting time signal course - second row. The image processing based on the time curve allows to extract qualitative or quantitative metrics of perfusion (DSC-MRI) and/or permeability (DCE-MRI) and obtain parametric maps.

NIH-PA Author Manuscript
NIH-PA Author Manuscript
NIH-PA Author Manuscript

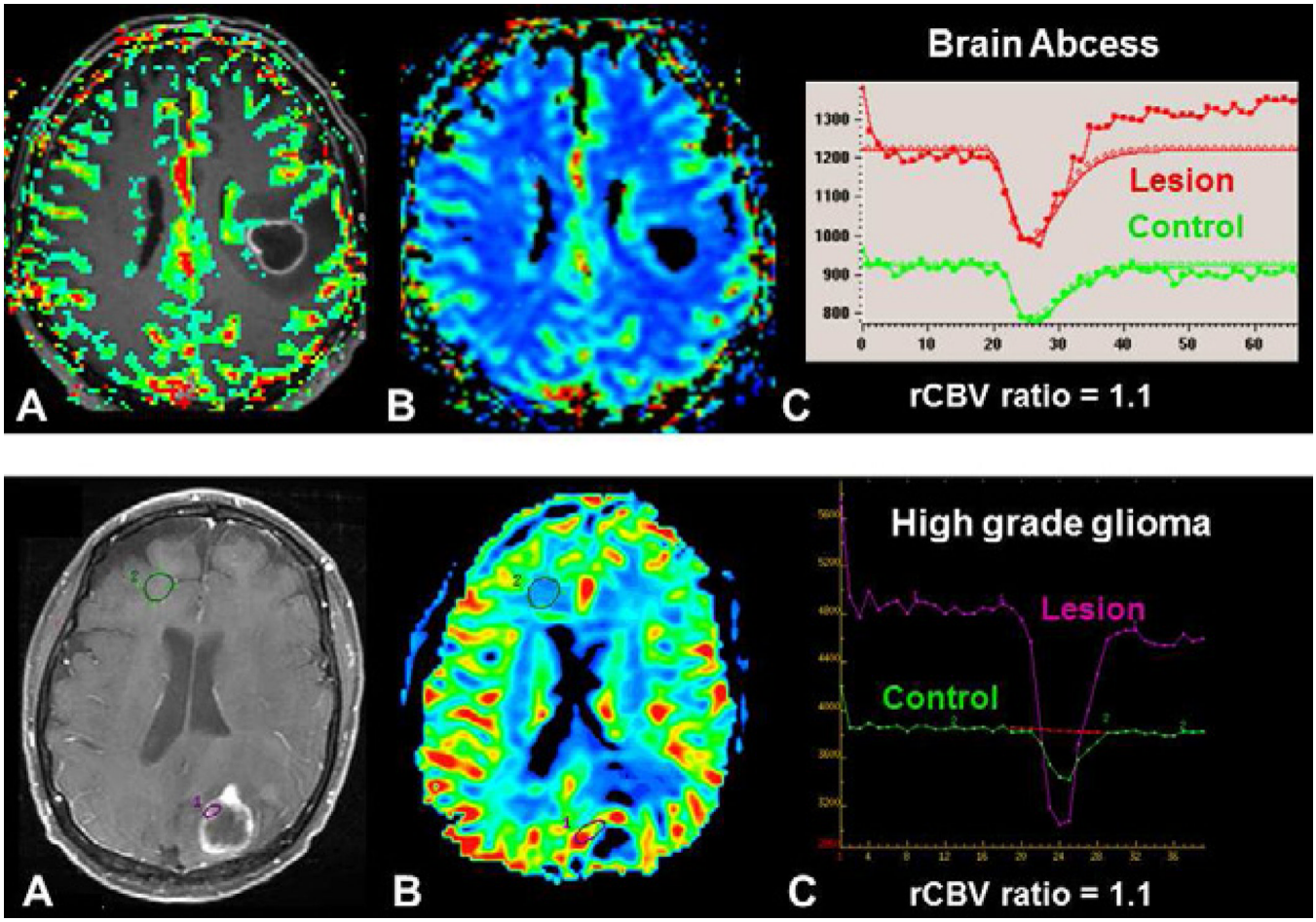

Fig. 2.

Differential diagnostic of brain tumor using DSC-MRI. Both patients presented with a mass demonstraing central necrosis and peripheral enhancement (A, D). In a brain abscess, (upper row) DSC-MRI demonstrates a low rCBV ratio (C) without visible increased perfusion on the rCBV color map (B), whereas in a brain tumor, in this case a metastasis, (lower row), DSC-MRI demonstrates an increase perfusion within enhanced parts of the lesion (E) with a high rCBV ratio (F).

NIH-PA Author Manuscript
NIH-PA Author Manuscript
NIH-PA Author Manuscript

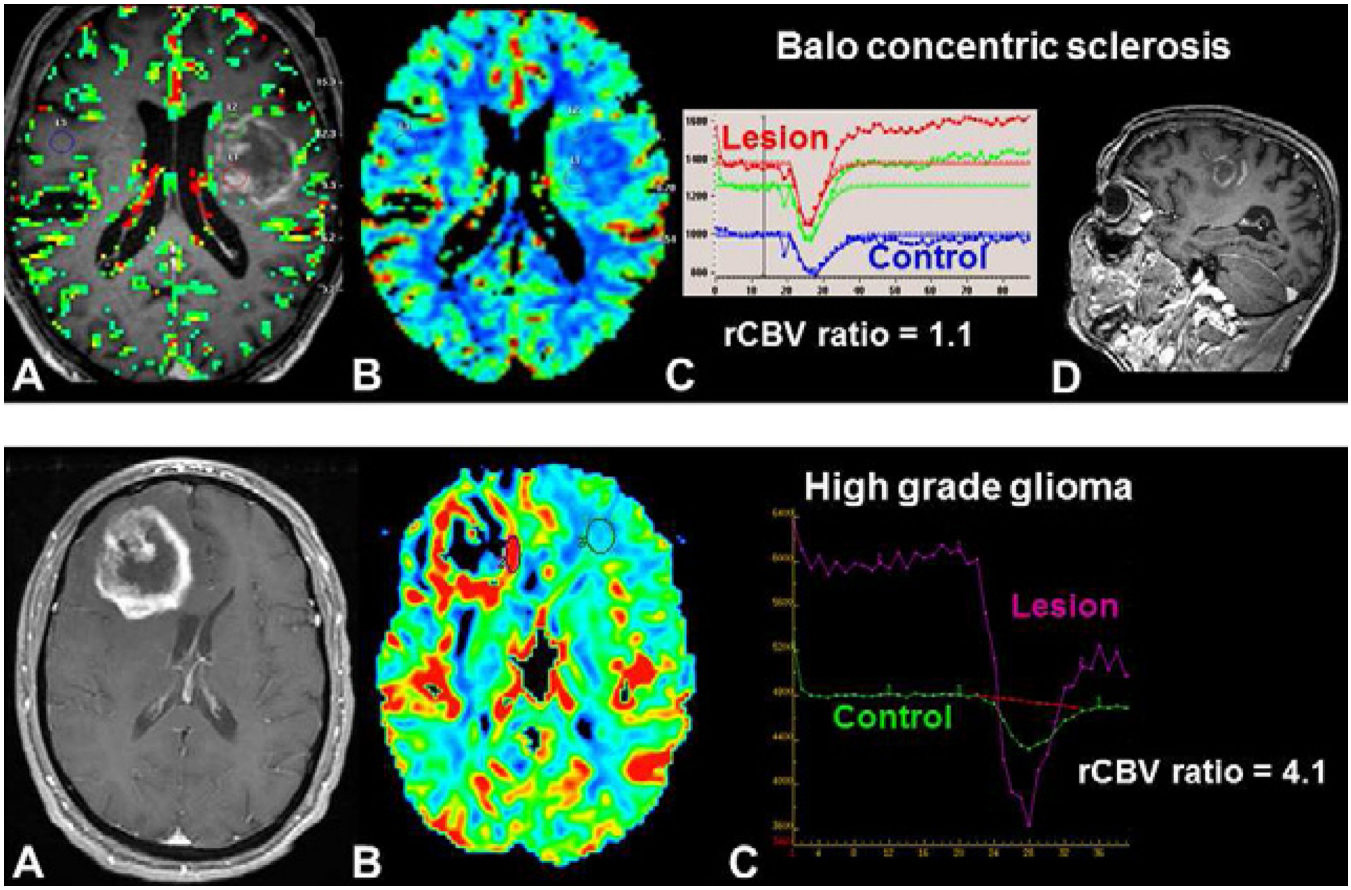

Fig. 3.

Differential diagnosis of an intracranial mass using DSC-MRI. Both patients presented with a peripherally enhancing, centrally necrotic mass (A, E). In Balo concentric sclerosis (upper row), DSC-MRI demonstrates a low rCBV ratio (C) without visible increased perfusion on the rCBV color map (B). Concentric enhancement of the lesion is seen on sagittal post-contrast T1-weighted image (D). In a high-grade glioma (lower row), DSC-MRI demonstrates increased perfusion within the enhancing portions s of the lesion (F) with a high rCBV ratio (G).

NIH-PA Author Manuscript
NIH-PA Author Manuscript
NIH-PA Author Manuscript

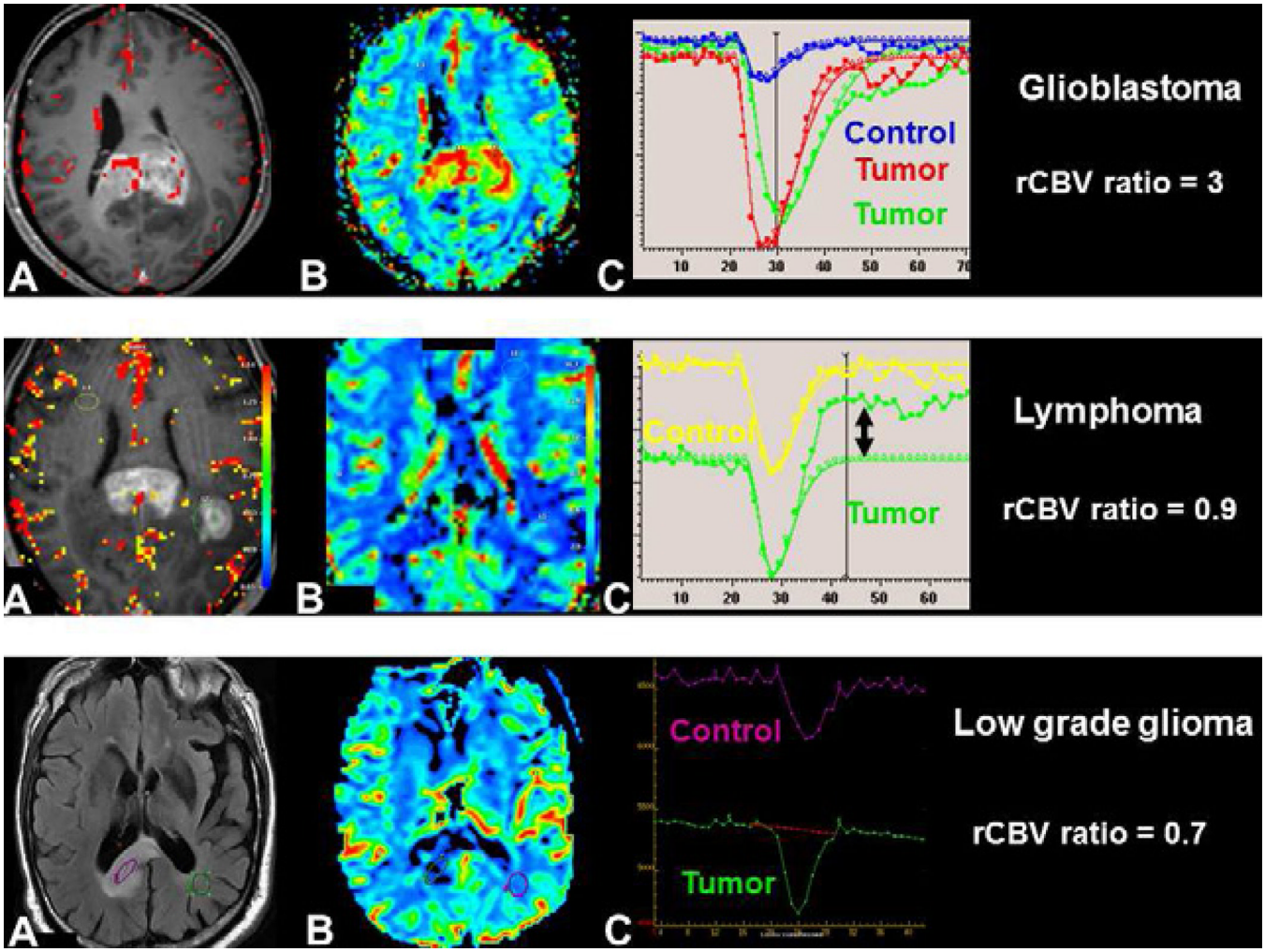

Fig. 4.

Differentiation of brain tumors involving the corpus callosum using DSC-MRI: glioblastoma (upper row), primary CNS lymphoma (middle row) and low-grade glioma (lower row). Contrast enhancement within the tumor seen on axial T1-weighted image post-gadolinium does not discriminate glioblastoma (A) from and lymphoma (D). rCBV color maps demonstrates increased perfusion within glioblastoma(B), but not within lymphoma (E). The rCBV ratio - tumoral rCBV /normal brain rCBV- is elevated (>1.75) for glioblastoma and low for lymphoma. The non-enhancing low-grade glioma, seen with increased signal on FLAIR images (G) has decreased perfusion on rCBV map (H) with a low rCBV ratio. Visual inspection of the curve demonstrates a high percentage signal recovery within lymphoma (F-double arrow), not visible for low grade glioma (I).

NIH-PA Author Manuscript
NIH-PA Author Manuscript
NIH-PA Author Manuscript

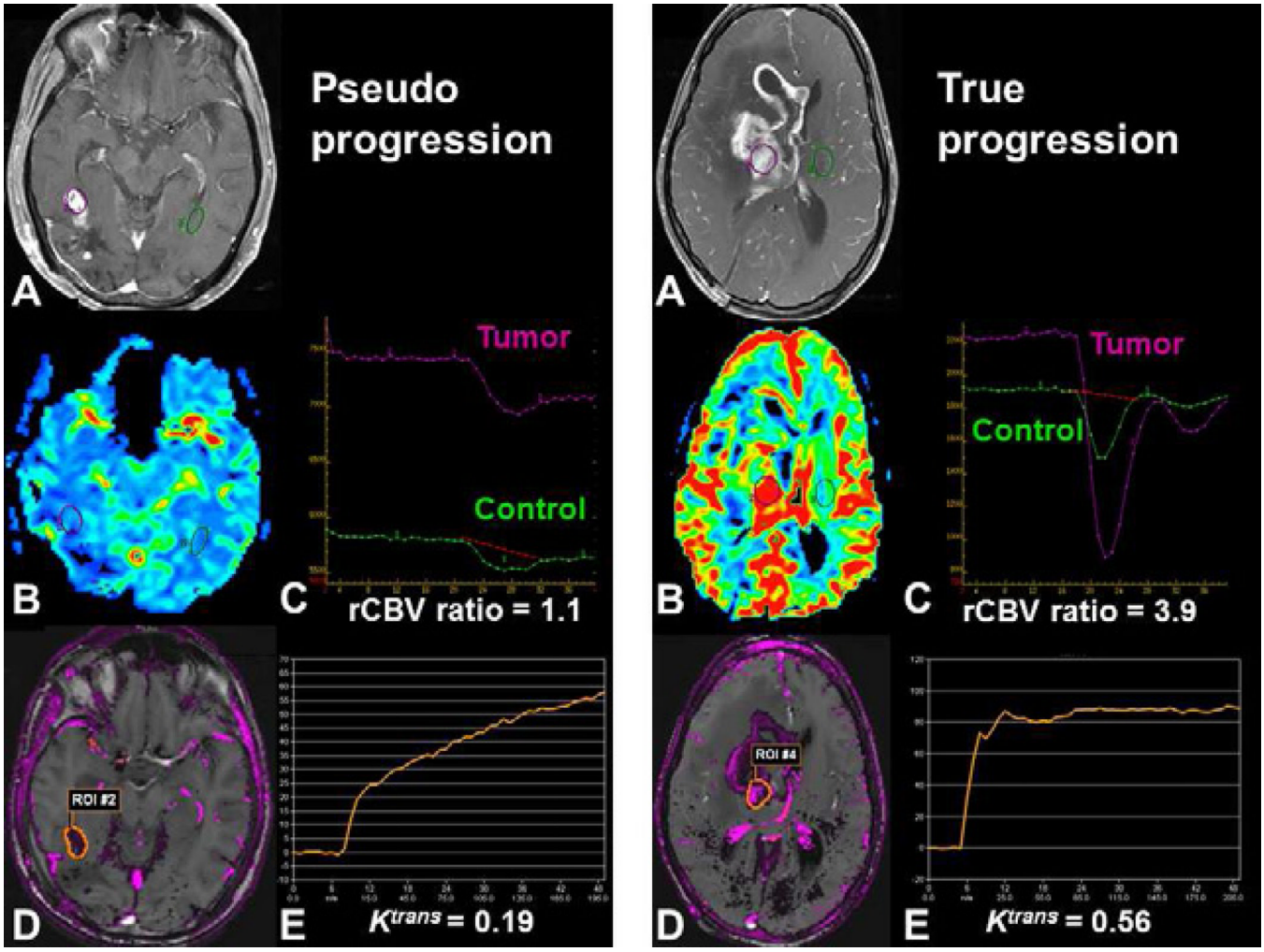

Fig. 5.

Post-therapeutic evaluation of high-grade glioma using DSC-MRI and DCE-MRI. Both patients demonstrate increased contrast enhancement 3 months following combined chemoradiotherapy with temozolomide. (A, F). Pseudoprogression may demonstrate decreased perfusion with a low rCBV ratio using DSC-MRI (B, C) and moderate vascular permeability (D, E) with a progressive enhancement (E) using DCE-MRI. True early progression may demonstrate increased perfusion with a high rCBV ratio (G, H) with high permeability and rapid enhancement (I, J).

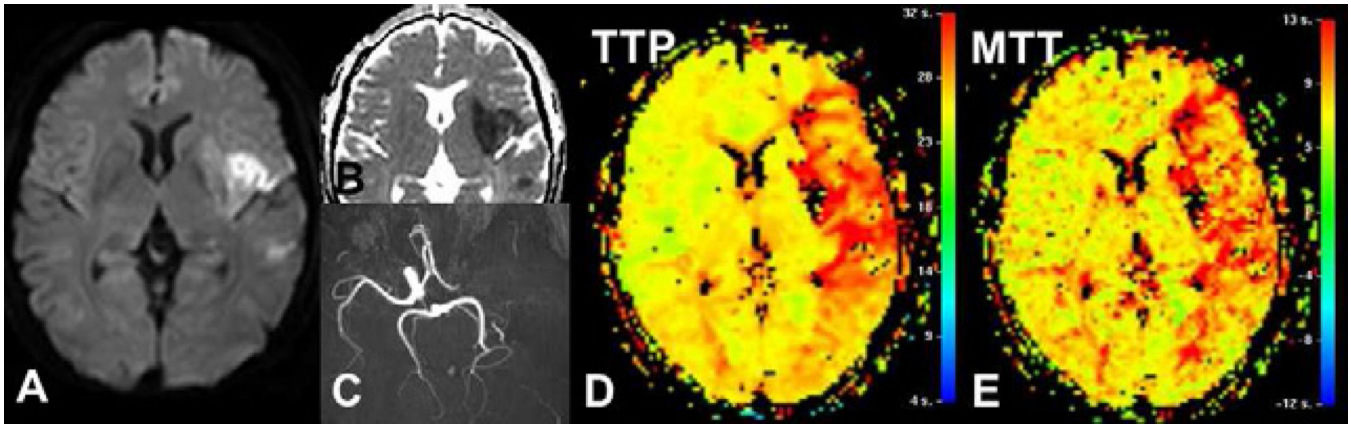

Fig. 6.

Acute ischemic stroke in left middle cerebral artery territory, due to a left internal carotid artery occlusion (C). Diffusion-weighted image (A) and ADC map (B) demonstrates an ischemic core smaller than the hypoperfused territory seen on TTP (D) or MTT (E) maps, as red area. The perfusion/diffusion mismatch – difference between these two volumes- is considered as the tissue at risk to infarction without arterial recanalization.

NIH-PA Author Manuscript NIH-PA Author Manuscript NIH-PA Author Manuscript